Anal Bioanal Chem (2015) 407:2095–2106
DOI 10.1007/s00216-014-8232-7

RESEARCH PAPER

A spiked tissue-based approach for quantification of phosphatidylcholines in brain section by MALDI mass spectrometry imaging

Laure Jadoul · Rémi Longuespée · Agnès Noël · Edwin De Pauw

Received: 1 September 2014 / Revised: 28 September 2014 / Accepted: 1 October 2014 / Published online: 19 October 2014

Abstract In the last few years, matrix-assisted laser desorption/ionization (MALDI) mass spectrometry imaging (MSI) has been successfully used to study the distribution of lipids within tissue sections. However, few efforts have been made to acquire reliable quantitative data regarding the localized concentrations of these molecules. Here we propose an approach based on brain homogenates for the quantification of phosphatidylcholines (PCs) in brain section by MALDI MSI. Homogenates were spiked with a range of PC(16:0 d31/18:1) concentrations. Sections from homogenates and intact brain were simultaneously prepared before being analyzed by MALDI MSI using a Fourier transform ion cyclotron resonance (FT-ICR) analyzer. Standard curves were generated from the signal intensity of the different PC(16:0 d31/18:1) ionic species ($[M+H]^+$, $[M+Na]^+$ and $[M+K]^+$) detected from the homogenate sections. Localized quantitative data were finally extracted by correlating the standard curves with the signal intensities of endogenous PC (especially PC(16:0/18:1)) ionic species detected on different areas of the brain section. They were consistent with quantitative values found in the literature. This work introduces a new method to take directly into account biological matrix effects for the quantification of lipids as well as other endogenous compounds, in tissue sections by MALDI MSI.

Keywords MALDI · Imaging · Lipids · Quantification

Abbreviations

a.u.	Arbitrary unit
H&E	Haematoxylin and eosin
ITO	Indium tin oxide
MALDI	Matrix-assisted laser desorption/ionization
MSI	Mass spectrometry imaging
PC	Phosphatidylcholine
R^2	Coefficient of determination
ROI	Region of interest

Introduction

Lipids play essential biological functions, such as composition of cell membranes, cell signalling and energy storage [1]. Alterations in lipid metabolism are related to different human diseases (e.g. diabetes, cancer and neurodegenerative diseases) [2–7]. Therefore, there is a growing interest to study lipids in biological samples with a special effort to map their distribution in various tissues.

In the last few years, matrix-assisted laser desorption/ionization (MALDI) mass spectrometry imaging (MSI) has emerged as a powerful tool to study the distribution of these biomolecules within tissue sections [8–17]. The major advantage of this technique is its ability to simultaneously detect and map specific lipid species without the requirement of probes or staining. In this context, high-resolution mass spectrometry analyzers (e.g. orbitrap and Fourier transform ion cyclotron resonance, FT-ICR) provide an invaluable support in the

Published in the topical collection *Mass Spectrometry Imaging* with guest editors Andreas Römpp and Uwe Karst.

Electronic supplementary material The online version of this article (doi:10.1007/s00216-014-8232-7) contains supplementary material, which is available to authorized users.

L. Jadoul (✉) · R. Longuespée · E. De Pauw (✉)
Mass Spectrometry Laboratory, Department of Chemistry, GIGA-Research, University of Liège, 4000 Liège, Belgium
e-mail: laure.jadoul@doct.ulg.ac.be
e-mail: e.depauw@ulg.ac.be

A. Noël
Laboratory of Tumor and Development Biology, GIGA-Cancer, University of Liège, 4000 Liège, Belgium

characterization of specific lipids by giving accurate mass measurements and high mass resolution [18, 19, 4].

However, MALDI MSI has not yet reached its full potential because efforts are still required to extract reliable quantitative information from MALDI MSI data. Quantification of a given analyte is difficult because the ion intensity recorded depends on (1) its concentration in the sample, (2) its particular ionization yield, (3) the matrix properties and deposition method and (4) the chemical and morphological environment that is sampled simultaneously with the analyte [20]. The latter is commonly known as ion suppression effects. During a MALDI imaging experiment, all these factors occur simultaneously in a complex manner that can influence ion intensities. Consequently, analyte(s) can be detected with different intensities depending on the analyte properties and tissue environment, even if they are present at identical concentrations.

Nevertheless, progresses have been made in the field of quantitative MALDI MSI analyses. Several methods have been developed to determine local concentrations of compounds (especially drugs) within tissue sections [20]. First, imaging data were generally normalized to take into account matrix application and ion suppression effects. To this end, an added compound or matrix peaks were usually used as an internal standard [21, 22]. A recently developed method relied on a tissue-specific normalization factor (called tissue extinction coefficient) to correct ion suppression effects [23]. A glass slide and a tissue section were simultaneously covered using an analyte-matrix mixture. The coefficient was calculated using the ratio between the analyte intensity recorded on the tissue section and on the glass slide. Secondly, imaging data were converted to analyte signal(s) into surface concentration(s). The ion intensity recorded on a dosed tissue section was usually compared to a calibration curve generated from standard dilution series spotted on (or below) the surface of control tissue section [21, 24, 25]. However, it was unlikely that the standard mimics crystallization, desorption and ionization of compounds initially found in the complex tissue samples. Recently, approaches based on the use of tissue homogenates spiked with different standard concentrations have also been reported [26, 27]. The signal intensity recorded on the dosed tissues was compared to a standard curve generated from the spiked homogenates in order to extract quantitative information. By incorporating the standard into homogenates, it was expected that the standard closely mimics the behaviour of compounds (initially present in the tissue) during the MALDI process. In several studies, orthogonal analyses (e.g. by LC-MS) were conducted in parallel to control quantitative MSI results [26, 23, 24, 28]. The correlation between these data sets supports the possibility of extracting quantitative information from MALDI MSI data.

Less attention has been given to the quantification of lipids within tissue sections. A study was conducted to investigate the relationship between the abundance of phosphatidylcholine (PC) species recorded by MALDI MSI and the relative amounts of PC species measured by LC-MS/MS in adjacent brain sections [29]. There was a good correlation between the relative quantitative information provided by MALDI MSI and LC-MS/MS. Considerations related to the quantification of lipids in nerve tissue have also been approached [30]. It included the investigation of the signal variability in successive MALDI MSI analyses as well as the comparison of three methods for applying an internal standard (a non-endogenous PC) to tissue sections. The standard was finally deposited using an inkjet printer under wet tissue in order to extract relative concentrations of endogenous PCs in the brain and spinal cord sections. The results were similar to data found in the literature.

As of today, no method has been yet reported to generate quantitative information on lipids present in tissue sections by MALDI MSI. Here we propose the use of brain homogenates spiked with PC(16:0 d31/18:1) to quantify endogenous PCs (especially PC(16:0/18:1)) in a mouse brain section. Brain tissues contain a large quantity of various lipid species, including PCs which are predominantly detected as positive ions during MALDI MSI analyses of brain sections [18]. In this work, brain homogenates were prepared and spiked with different PC(16:0 d31/18:1) concentrations. They were used to generate standard curves each corresponding to a specific PC(16:0 d31/18:1) ionic form (i.e. protonated, sodium or potassium adducts). Quantitative information on different PC ionic forms was finally extracted using these curves.

Material and methods

Chemicals

Methanol (MeOH, HPLC grade) was purchased from Biosolve (Valkenswaard, Netherlands). Ethanol (EtOH, absolute) and *o*-xylol (purity 99 %) were purchased from Thermo Fisher Scientific (Waltham, USA). Eosin Y and haematoxylin solution (modified according to Gill III) was purchased from Merck (Darmstadt, Germany). Chloroform ($CHCl_3$, purity ≥99.9 %) and 1,5-diaminonaphthalene (1,5-DAN, purity 97 %) were purchased from Sigma-Aldrich (St. Louis, USA).

Lipid standard

PC(16:0 d31/18:1) (1-palmitoyl-d31-2-oleoyl-*sn*-glycero-3-phosphocholine) was purchased from Avanti Polar Lipids, Inc. (Alabaster, USA). Lipid standard was used without further purification. Stock solution was prepared using a MeOH/$CHCl_3$ mixture (50/50 *v*/*v*) at a concentration of 45.46 mg/mL. Additional standard solutions were prepared

using a MeOH/$CHCl_3$ mixture (50/50 *v*/*v*) at concentrations of 0.57, 1.48, 2.79, 5.73, 14.45, 27.95 and 44.55 mg/mL.

Brain samples

BALB/c mouse was provided by the Central Animal Housing of the University of Liège. Pig brains of controlled origin were provided by a slaughterhouse. Tissues were collected before being snapped frozen by immersion in pre-cooled isopentane at −50 °C and stored at −80 °C. All subsequent sample handlings were made in dry ice. Experimentations were conducted in conformity with the ethics commission for animals use in the University of Liège.

Brain homogenates

Tissues were removed from the freezer and placed at −4 °C during 1 h. Pig brains were then homogenized using (1) a Potter-Elvehjem tissue grinder A 966 driven by a rotor (until complete homogenization; Thomas Scientific, Swedesboro, USA); (2) an ultrasonic homogenizer (ViBro Cell; Van Der Heyden, Brussels, Belgium); (3) a T 10 basic Ultra-Turrax mixer (30,000 rpm until complete homogenization; IKA-Werke, Staufen, Germany); or (4) a MagNA Lyser instrument (at 4500*g* during 30 s; Roche, Basel, Switzerland). In the latter case, tissues were placed in 2-mL tubes filled with ceramic beads before being homogenized. Homogenates were then collected using a 100-μL pipette before being transferred into 0.6-mL micro-tubes (Axygen, Tewksbury, USA). Conical extremity of pipette tips has been cut to facilitate the collection. The micro-tubes containing the homogenates were immersed in pre-cooled isopentane at −50 °C. These handlings were conducted in a cold room at −4 °C.

Incorporation of the lipid standard in brain homogenates

One hundred-microlitre standard solutions (prepared at different concentrations) were transferred by pipetting in the micro-tubes containing the tissue homogenates. The standard solutions were incorporated in the tissue homogenates using a Vortex-Genie 2 instrument (USA Scientific, Inc., Ocala, USA) and an Intelli-Mixer instrument (F64 at 99 rpm; ELMI Ltd., Riga, Latvia). The micro-tubes containing the homogenates were immersed in pre-cooled isopentane at −50 °C. These handlings were conducted in a cold room at −4 °C.

Tissue sectioning and coating

The micro-tubes containing the homogenates were removed from the freezer. The conical extremities of the micro-tubes were cut. The tissue homogenates were extracted from the micro-tubes by pushing them with a tweezers. These handlings were made in dry ice.

Each sample was mounted onto a sample holder using optimal cutting temperature media (Thermo Scientific, Waltham, USA). Samples were cut into 14-μm-thick sections using a cryostat Microm HM 500 O (Microm, Heidelberg, Germany). The temperatures of the sample holder and the razor blade were −45 and −35 °C for the spiked tissue homogenates and −12 and 20 °C for other tissue samples, respectively. Sections were thaw-mounted onto indium tin oxide (ITO)-coated glass slides (Bruker Daltonics, Bremen, Germany) before being placed for drying in a vacuum desiccator for about 1 h. When the intact brain was cut, coronal sections were prepared. Haematoxylin and eosin (H&E) staining was conducted on serial tissue sections.

The application of the 1,5-DAN matrix was conducted using a home-made sublimation device, as previously reported [11, 31]. The matrix powder (300 mg) was added to the bottom section of the apparatus. The ITO-coated glass slides were fixed in a flat-bottom condenser using a thermally conductive tape. The condenser was assembled with the bottom section of the apparatus. The apparatus was then placed under a vacuum during approximately 10 min. The ITO-coated glass slide was cooled (via the condenser) at 3–4 °C during 5 min. A sand bath was finally used to heat the matrix at 140 °C during 5 min.

Tissue staining

Tissue sections were stained with H&E. Sections were successively immersed in 100 % EtOH (8 s), 90 % EtOH (8 s), 70 % EtOH (8 s) and distilled water (4 s). They were then stained by immersion in a haematoxylin Gill III solution during 2 min. Sections were washed using HCl 0.1 % (2 s) and running water (3 min). They were then stained by immersion in an eosin solution (1 min) before being washed using distilled water (4 s). Sections were successively immersed in 70 % EtOH (4 s), 90 % EtOH (4 s), 100 % EtOH (4 s) and two xylol baths (10 min).

Microscope examinations have been conducted using an IX81 inverted microscope (Olympus, Tokyo, Japan). The cellSens 1.9 software was used to control the microscope and measure the surface of regions observed on the tissue sections. For histological comparison, we used a reference atlas provided by the Allen Institute for Brain Science (Allen Brain Atlas: data portal, http://www.brain-map.org/).

MALDI mass spectrometry imaging analysis

MALDI MSI analyses were conducted using a SolariX FTMS 9.4-T mass spectrometer (Bruker Daltonics, Bremen, Germany). The mass spectra were acquired at each position in positive ion mode using the following settings: a laser frequency of 1 kHz, a number of laser shots of 2000, a number of acquired scan of 1, a mass range from *m*/*z* 100 to 1500 and a

laser power of 20 %. Settings were tuned on a sample containing four lipid standards [PC(16:0/14:0), PC(18:0/18:1), PE(16:0/18:1) and PE(18:0/18:1)] (Avanti Polar Lipids, Inc., Alabaster, USA). This sample was also used to calibrate the instrument considering the different ionic forms (protonated and salt adduct species) detected. We used different lateral resolutions during this work that are further specified in the text. SolariX Control 1.5.0 and FlexImaging 3.0 software (Bruker Daltonics, Bremen, Germany) were used to control the instrument and to set imaging parameters, respectively. The latter was also used to visualize molecular images using a 0.005-Da mass filter. Assignment of the *m/z* values to lipid species has been conducted using LIPID MAPS database (The LIPID MAPS Lipidomics Gateway, http://lipidmaps.org/) and data reported in the literature [32–35, 10].

Data treatment

The scaling factor (RMS normalization method) provided by FlexImaging 3.0 software was usually not used to normalize data because it might cause potential artefacts and lead to misleading results in our experimental conditions [36]. If this scaling factor was used, it will be specified in the text. Details about the calculation of quantitative data will be also further detailed in the text.

Results and discussion

Morphology of tissue homogenates

A protocol to prepare tissue homogenates was first developed. To this end, we compared the influence of different preparation conditions on tissue morphology.

First, pig brains were homogenized using several homogenization devices: (1) a Potter-Elvehjem instrument, (2) an ultrasonic homogenizer, (3) a tissue mixer and (4) a MagNA Lyser instrument. Sections from an intact mouse brain and homogenates were then stained with H&E (Fig. 1a–e).

The quality of the sections was influenced by the homogenization conditions. We observed damages (e.g. holes) on the sample surface when the ultrasonic homogenizer and the tissue mixer were used. Such damages did not occur using the Potter-Elvehjem and the MagNA Lyser instruments. The homogenization systems also influenced the texture of the samples. The ultrasonic homogenizer and the tissue mixer formed clusters of cell nuclei across the sample surface. In contrast, the morphology of the homogenates was similar at any point on the section surface when the Potter-Elvehjem and the MagNA Lyser instruments were used. When we

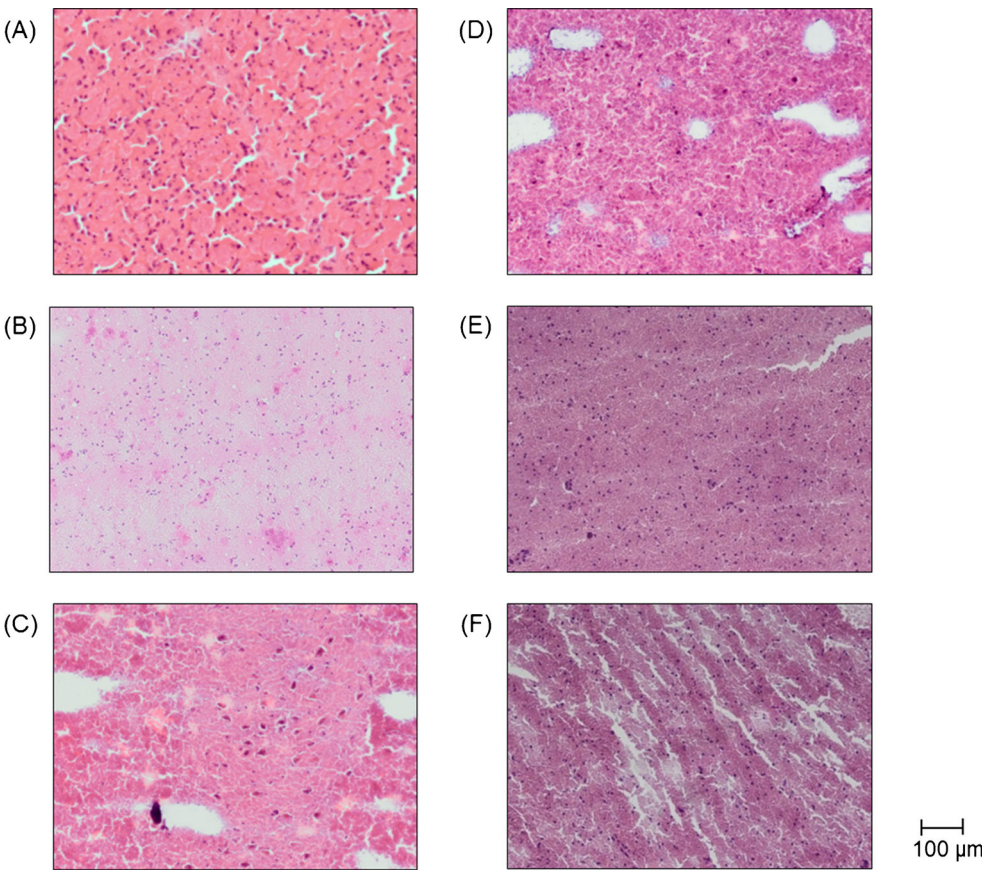

Fig. 1 H&E-stained sections from (**A**) an intact brain and (**B**–**F**) brain homogenates prepared using different conditions. Four homogenization devices: (**B**) a Potter-Elvejhem, (**C**) an ultrasonic probe, (**D**) a mixer and (**E**) a MagNA Lyser. Two freezing methods: (**E**) micro-tubes that were immersed in pre-cooled isopentane and (**F**) micro-tube that was placed in an ultra-cold freezer at a temperature of −80 °C

compared the intact brain section with the homogenate sections, we observed the similar number and distribution of cell nuclei across the homogenates prepared using the Potter-Elvehjem and the MagNA Lyser instruments.

It was important that the tissue homogenates and the intact tissue were closed regarding their morphology. This similarity ensures comparable analyte-matrix interactions, analyte extraction, analyte desorption and analyte ionization between the intact and the homogenate samples. It is an essential requirement before conducting further comparison of signal intensities recorded on both samples. Based on our observations, the Potter-Elvehjem and the MagNA Lyser appeared suitable for the preparation of tissue homogenates. We chose to use the Potter-Elvehjem in the rest of this study because of its ease of use for the homogenization of large quantities of material (in the range of grams; e.g. pig brain).

Secondly, two freezing methods were compared. Pig brains were homogenized using the MagNA Lyser instrument before being frozen by (1) the storage of the micro-tubes containing the homogenates in an ultra-cold freezer at −80 °C and (2) the immersion of the micro-tubes in pre-cooled isopentane at −50 °C before being placed at −80 °C. Sections were then stained with H&E (Fig. 1e, f).

The freezing process results in the formation of ice crystals, which tend to increase in size over time. The freezing speed has a direct influence on ice crystal size. The freezing process was faster using the pre-cooled isopentane than using the ultra-cold freezer. Use of pre-cooled isopentane prevented tissue damages due to crystal formation, which can be observed on the images corresponding to the direct storage at 80 °C in an ultra-cold freezer [37]. Similar observations were made comparing the two freezing methods using tissue homogenates prepared with the Potter-Elvehjem. This is in agreement with previous studies on tissue preservation. In the rest of this study, homogenates were therefore frozen by an immersion in pre-cooled isopentane.

Distribution of endogenous PCs within tissue homogenates

Pig brains were homogenized using the Potter-Elvehjem instrument. A homogenate section was prepared and transferred onto an ITO-coated glass slide. The section was covered with the matrix before being analysed by MALDI MSI (Fig. 2). Different PC species were detected everywhere across the homogenate section surface, as illustrated for PC(16:0/18:1) (Fig. 2b). Only light differences of signal intensity were observable on the MALDI images. However, those were not significant compared to differences that may be observed for various regions of interest (ROIs) on a non-homogenized brain tissue section, and were only obvious for the most intense ionic specie ($[PC(16:0\ d/18:1)+K]^+$). Consequently, endogenous PCs appeared to be relatively homogeneously distributed within the tissue homogenates resulting from the use of the Potter-Elvehjem instrument. In this paper, we used two different monochromatic colour scales to clearly identify the results that correspond to the endogenous PC(16:0/18:1) (in red) and to the standard PC(16:0 d31/18:1) (in green), respectively.

We also compared the average mass spectra recorded on sections from a pig brain homogenate and an intact mouse brain (see Electronic supplementary material, Fig. S-1). It appeared that the lipid signature detected on both samples was closely similar. We noted that the homogenization process did not change the chemical composition of the tissue. In the rest of this study, we used pig brain to prepare spiked tissue homogenates because of the availability of a sufficient amount of tissue, which was required to prepare homogenate samples.

Distribution of PC(16:0 d31/18:1) within tissue homogenates

During this work, we focused on the quantification of PC(16:0/18:1), which is an endogenous lipid predominantly present in brain tissues [35]. An important factor to consider was that the standard and the targeted analyte(s) shared a common molecular structure. In order to warrant specific ionization efficiency, it was essential to ensure that the standard was extracted, desorbed and ionized in the same manner as the analyte(s). The standard PC(16:0 d31/18:1) was

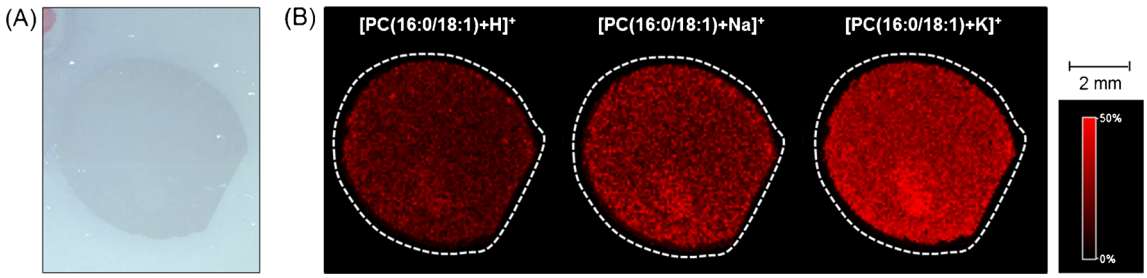

Fig. 2 Analysis by MALDI MSI of a brain homogenate section. (**A**) Optical image of the section. (**B**) Molecular images showing the distribution of PC(16:0/18:1) ionic species across the section surface. Lateral resolution=80 μm

selected because its molecular structure was similar to the endogenous PC(16:0/18:1). Moreover, in results of the analyses of tissue homogenates, we detected no ionic signal that was likely to interfere with the *m/z* values corresponding to $[PC(16:0\ d31/18:1)+H]^+$, $[PC(16:0\ d31/18:1)+Na]^+$ and $[PC(16:0\ d31/18:1)+K]^+$ ionic species.

Pig brain was homogenized using the Potter-Elvehjem instrument. We spiked this homogenate with a known amount of PC(16:0 d31/18:1). Sections from the spiked homogenate and the blank homogenate were prepared and transferred onto a single ITO-coated glass slide. We applied the matrix on the sample surface before starting the analysis by MALDI MSI (Fig. 3). The intensities corresponding to the different PC(16:0 d31/18:1) ionic forms ($[M+H]^+$, $[M+Na]^+$ and $[M+K]^+$) were relatively constant across the surface of the sections (Fig. 3d). Using our incorporation method, PC(16:0 d31/18:1) was homogeneously distributed within the homogenate sample surface.

When comparing the signal intensities of endogenous PCs recorded within the blank homogenate and the spiked homogenate, we did not observe significant intensity changes after standard incorporation, as illustrated for the PC(16:0/18:1) potassium adduct in Fig. 3b, d. Hence the addition of PC(16:0 d31/18:1) in the homogenate did not change the signal intensities of endogenous PCs (e.g. PC(16:0/18:1)).

Finally, we verified the potential influence of solvent addition on the morphology of the standard spiked homogenates. We compared the structure of the spiked and the non-spiked homogenates and observed no structural difference on the homogenate surfaces due to solvent addition (data not shown).

Addition of different PC(16:0 d31/18:1) concentrations in tissue homogenates

A set of tissue homogenates was spiked with a range of PC(16:0 d31/18:1) concentrations. For each concentration, three serial sections were transferred onto an ITO-coated glass slide. The sections were analysed by MALDI MSI after the deposition of matrix (Fig. 4a). We then defined ROIs around each homogenate sections. In this way, FlexImaging 3.0 software generated ROI-specific average mass spectra. We then manually reported the ion intensities of each average mass spectrum. We especially took into account the intensities of the monoisotopic peaks corresponding to $[PC(16:0\ d31/18:1)+H]^+$, $[PC(16:0\ d31/18:1)+Na]^+$ and $[PC(16:0\ d31/18:1)+K]^+$ species. For each concentration, an average intensity value was calculated from the three serial sections. A standard curve was finally generated for each ionic form by plotting these values as a function of the quantities of standard incorporated into tissue homogenates (Fig. 4b, c). In MALDI MSI experiments, PCs are usually detected as protonated and adducted (i.e. sodium and potassium) ions. Sodium and potassium are naturally present in the biological sample where they act as buffering salts in cellular fluids [29]. The gradient of Na^+ and K^+ concentrations is maintained across the cell membranes. The abundance of the ion forms detected by MALDI MSI within a tissue section is likely to change depending on the availability of the alkali metal salts in the sample.

A simple linear regression was used to model the relationship between the intensity values and the quantity of PC(16:0 d31/18:1) spiked in tissue homogenates. The coefficients of determination (R^2) of $[PC(16:0\ d31/18:1)+H]^+$, $[PC(16:0\ d31/18:1)+Na]^+$ and $[PC(16:0\ d31/18:1)+K]^+$ were 0.9500, 0.9461 and 0.9638, respectively. We did not observe significant differences between the R^2 values of the different ionic species. However, the linear regression equations were different. It appeared to be essential to treat independently data from the different ionic forms. Quantitative data of $[M+H]^+$, $[M+Na]^+$ and $[M+K]^+$ lipid ionic forms should be extracted from the standard curve generated from $[PC(16:0\ d31/18:1)+H]^+$, $[PC(16:0\ d31/18:1)+Na]^+$ and $[PC(16:0\ d31/18:1)+K]^+$,

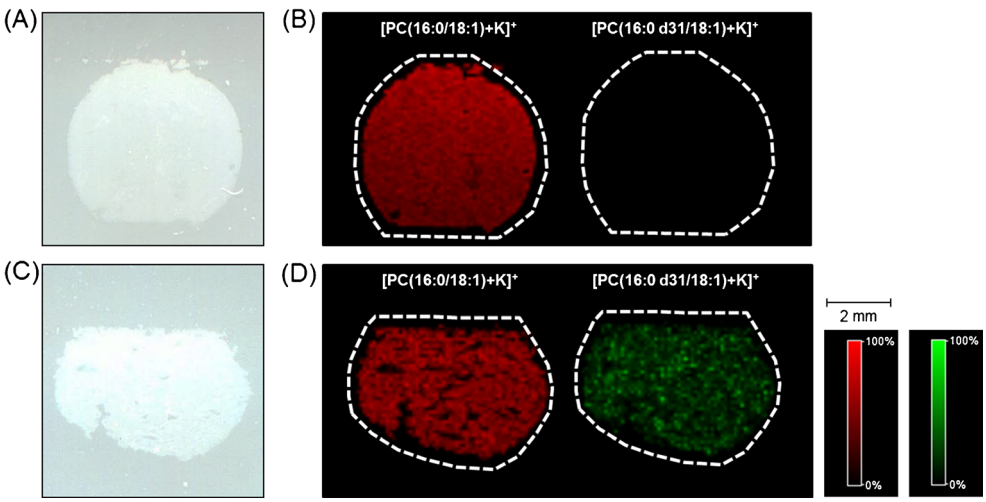

Fig. 3 Analysis by MALDI MSI of sections from (**A**, **B**) a blank homogenate and (**C**, **D**) a spiked homogenate (with 5000 μg/g of PC(16:0 d31/18:1)). (**A**, **C**) Optical images of the sections. (**B**, **D**) Molecular images showing the distribution of $[PC(16:0/18:1)+K]^+$ (*red*) and $[PC(16:0\ d31/18:1)+K]^+$ (*green*) across the section surfaces. Lateral resolution= 100 μm

respectively. When we considered the sum of the intensity values of the three species, the R^2 value became 0.9539. Data showed a relatively good linearity over 3 orders of magnitude. Based on these observations, we considered that this model was suitable for our future applications. The standard deviation (SD) and the relative standard deviation (RSD) were calculated (Electronic supplementary material, Table S-1).

We investigated the influence of the scaling factor provided by FlexImaging 3.0 software on the data set. We analysed tissue homogenates in which compounds were homogeneously distributed (Fig. 2b). However, PC(16:0/18:1) was here detected with different intensities from a homogenate section to another (Electronic supplementary material, Fig. S-2b). It was probably due to the matrix application step. When considering the optical scan, it appeared that the matrix layer was inhomogeneous (Electronic supplementary material, Fig. S-2a). The amount of matrix influenced the lipid desorption/ionization efficiency. For example, PC(16:0/18:1) was more intensely detected within homogenate sections covered with more matrix (Electronic supplementary material, Fig. S-2a, b). The application of the scaling factor allowed for the generation of more homogenous PC(16:0/18:1) images (Electronic supplementary material, Fig. S-2c). We generated standard calibration curves from normalized intensity values (Electronic supplementary material, Fig. S-2d). R^2 values of $[PC(16:0\ d31/18:1)+H]^+$, $[PC(16:0\ d31/18:1)+Na]^+$ and $[PC(16:0\ d31/18:1)+K]^+$ were 0.9991, 0.9986 and 0.9985, respectively. The R^2 value corresponding to the sum of the different ionic species was 0.9994. Consequently, the data normalization improved here the linearity of our data set as well as its variability (Electronic supplementary material, Table S-2).

Normalization algorithms can produce artefacts that mainly result from the inhomogeneous presence of peaks with

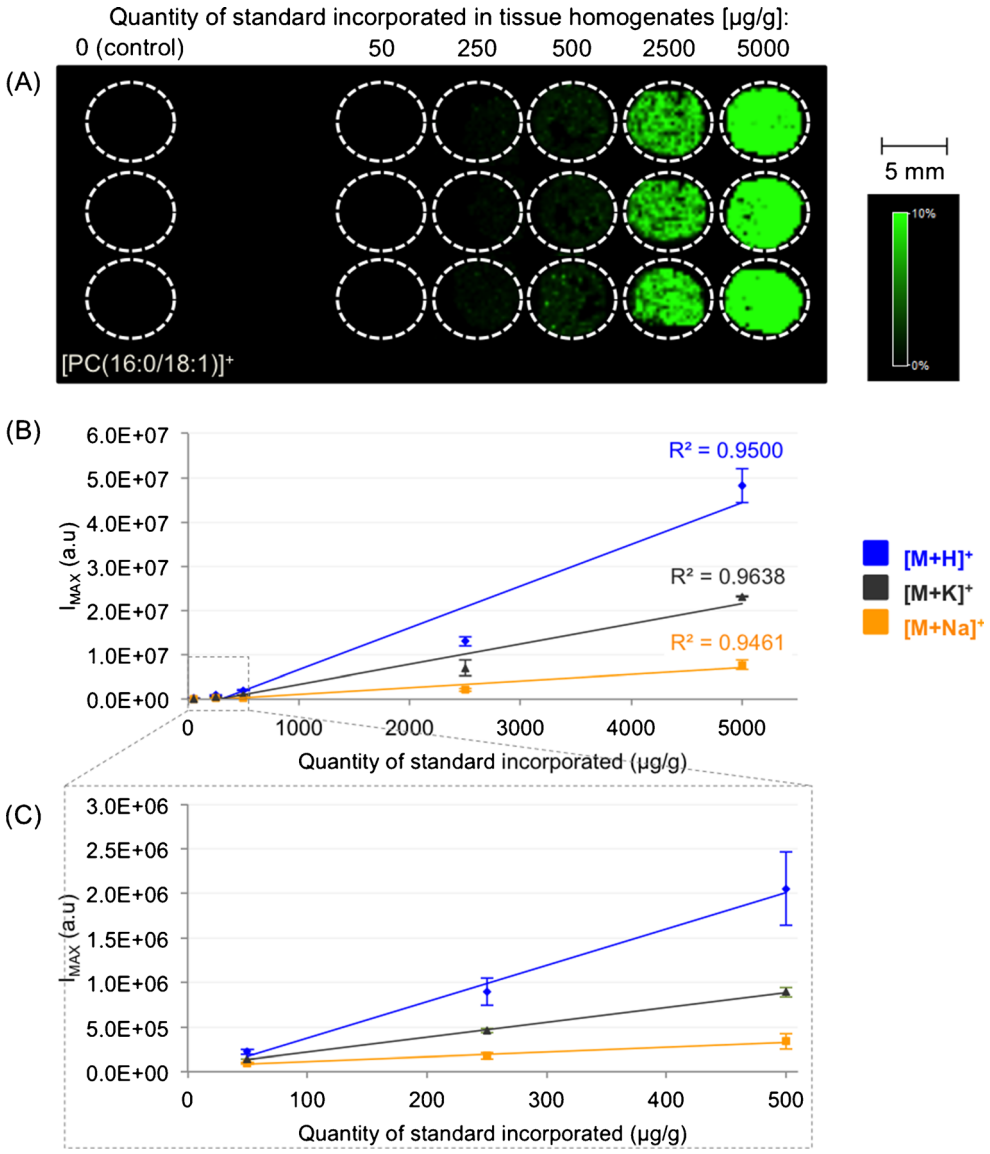

Fig. 4 Analysis by MALDI MSI of brain homogenate sections spiked with a range (between 5 and 5000 µg/g) of PC(16:0 d31/18:1) concentrations. (**A**) Molecular image showing the distribution of $[PC(16:0\ d31/18:1)+H]^+$ across the section surfaces. (**B**) Standard curves generated by plotting the intensity values of the different PC(16:0 d31/18:1) ionic species ($[M+H]^+$, $[M+Na]^+$ and $[M+K]^+$) as a function of the quantities of PC(16:0 d31/18:1) added to the homogenates. (**C**) Zoomed view on the standard curves. *Error bars* corresponded to the SD values. Lateral resolution=255 µm

unusual high intensities or areas [36]. This is typical when heterogeneous tissues were analysed because major compounds can be detected with high intensities in specific areas. These artefacts can lead to wrong data interpretations. During this experiment, we analysed tissue homogenates in which compounds were homogeneously distributed (Fig. 2b). The application of the scaling factor was therefore unlikely to produce such artefacts. It takes into account the variations of peak intensities due to the inhomogeneity of the matrix layer and corrected the data. Below in this paper, we analysed not only homogenate sections but also an intact brain section, which is a heterogeneous and structured tissue. That is why we chose to show unprocessed data in the rest of the paper. However, the normalized data can be found in the Electronic supplementary material.

Quantification of endogenous PCs in brain section

A set of brain homogenates were spiked with a range of different PC(16:0 d31/18:1) concentrations. Sections were transferred on an ITO-coated glass slide next to an intact brain section. Sections were analysed by MALDI MSI after the application of the matrix (Fig. 5). We defined ROIs around each section in order to generate ROI-specific average mass spectra. We reported the average intensities of the $[PC(16:0\ d31/18:1)+H]^+$, $[PC(16:0\ d31/18:1)+Na]^+$ and $[PC(16:0\ d31/18:1)+K]^+$ monoisotopic peaks recorded on each average mass spectrum in order to generate standard curves (Fig. 5c). The R^2 values of these curves were 0.9898, 0.9919 and 0.9942, respectively. These values were higher than the R^2 values of earlier reports in this work (for non-normalized data). This was probably due to a more homogenous application of the matrix on the sample surface, as observed on the optical image of the ITO-coated glass slide on which the sections were deposited (data not shown). The standard curves were finally used to convert the signal intensity of the endogenous PC(16:0/18:1) into a concentration (in µg/g, Fig. 5d). To this end, the intensities of $[PC(16:0/18:1)+H]^+$, $[PC(16:0/18:1)+Na]^+$ and $[PC(16:0/18:1)+K]^+$ monoisotopic peaks were compared to the standard curves specific to each ionic form. Regarding the weight of the brain section, we determined the quantity of PC(16:0/18:1) species present within the whole surface of the

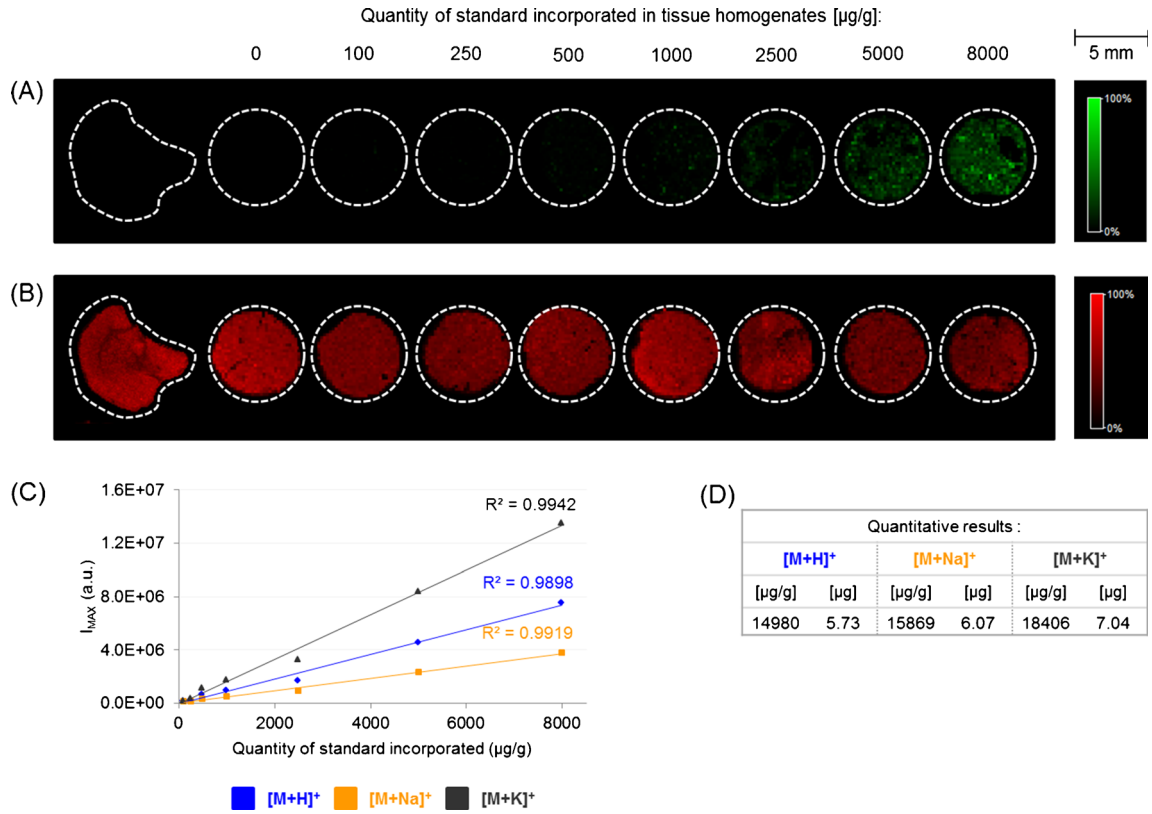

Fig. 5 Analysis by MALDI MSI of sections from an intact brain and brain homogenates spiked with a range (between 100 and 8000 µg/g) of PC(16:0 d31/18:1) concentrations. (**A**) Molecular image showing the distribution of $[PC(16:0\ d31/18:1)+H]^+$ across the section surfaces. (**B**) Molecular image showing the distribution of $[PC(16:0/18:1)+H]^+$. (**C**) Standard curves generated by plotting the intensity values of the different PC(16:0 d31/18:1) ionic species ($[M+H]^+$, $[M+Na]^+$ and $[M+K]^+$) as a function of the quantities of PC(16:0 d31/18:1) added to the homogenates. (**D**) Quantitative data obtained by correlating the intensity values of the different PC(16:0/18:1) ionic species with the standard curves

sample (in μg, Fig. 5d). The weight of the tissue section was approximately 383.50 μg. This value was determined by (1) simultaneously weighing serial tissue sections and (2) dividing the total mass by the number of weighing sections. All the quantitative data were consistent with the data already reported in the literature [38–40].

Several endogenous PC species were detected during this analysis. The different PC species shared a similar molecular structure. It was reasonable to assume that PCs were similarly extracted, desorbed and ionized during this MALDI MSI analysis. Based on this assumption, the standard curves generated from the PC(16:0 d31/18:1) standard could also be applied to extract a quantitative information for other PCs. As before, we reported the intensity values of other PC species (i.e. PC(18:0/18:1) and PC(16:0/16:0)) recorded on the whole brain section with the standard curves in order to extract quantitative data (in μg/g and μg, Table 1). It is known that other PL families (e.g. phosphatidylethanolamines or phosphatidylinositols) behave differently during the MALDI process [41]. The quantification of these compounds will probably require the use of standards with molecular structures close to the targeted lipid families.

MALDI MSI analysis highlighted localized variations of the signal intensity of PC species across the surface of the brain section (Fig. 6c). Based on the H&E staining of a serial section, we identified specific histological tissue structures that correlated with these variations (Fig. 6b, c). ROIs were defined on the molecular image according to these structures. Average mass spectra were generated for each structure. From these spectra, we reported the intensity values of the monoisotopic peaks corresponding to different PC ionic species, including $[PC(16:0/18:1)+H]^+$, $[PC(16:0/18:1)+Na]^+$ and $[PC(16:0/18:1)+K]^+$. We determined localized concentrations by comparing these values with the standard curves previously generated from the spiked tissue homogenates analysed simultaneously (in μg/g, Table 1). The surface areas of the whole tissue section, as well as of the specific tissue structures, were then determined using the cellSens 1.9 software. We calculated ratios between the surface areas of these structures and the surface area of the whole section. Regarding these ratios and the weight of the whole section, we calculated the weights of the different tissue structures. We were therefore able to calculate the quantity of PC species found within the different structures of the brain section (in μg, Table 1).

The scaling factor provided by FlexImaging 3.0 software was applied on the data set. We generated standard curves from the average intensities of $[PC(16:0\ d31/18:1)+H]^+$, $[PC(16:0\ d31/18:1)+Na]^+$ and $[PC(16:0\ d31/18:1)+K]^+$ monoisotopic peaks recorded on each spiked homogenate section. The R^2 values were 0.9934, 0.9937 and 0.9930, respectively. The normalization improved to a certain extent the linearity of the data set. However, this improvement was less significant than the data earlier reported in this work. This was probably due to a more homogeneous matrix application on the sample surface, as observed on the optical image (data not shown). In the same way as above, we generated quantitative data for different PC ionic species by correlating their normalized intensity values with these calibration curves (see Electronic

Table 1 Quantitative data calculated for different PC ionic species ($[M+H]^+$, $[M+Na]^+$ and $[M+K]^+$) across the whole brain section and on specific ROIs defined on the intact brain section surface

Assignment	Area	$[M+H]^+$		$[M+Na]^+$		$[M+K]^+$	
		μg/g	μg	μg/g	μg	μg/g	μg
PC(16:0/18:1)	Whole brain	14,980	5.73	15,869	6.07	18,406	7.04
	ROI1	10,603	0.15	9130	0.13	13,299	0.19
	ROI2	15,303	1.97	16,758	2.15	20,118	2.58
	ROI3	16,121	0.34	20,891	0.44	19,963	0.42
	ROI4	13,872	1.19	14,213	1.22	17,016	1.46
	ROI5	17,757	0.58	17,712	0.58	22,600	0.74
PC(18:0/18:1)	Whole brain	6347	2.43	14,827	5.67	46.42	1.78
	ROI1	6724	0.10	9294	0.13	5289	0.08
	ROI2	5567	0.71	13,407	1.72	4539	0.58
	ROI3	6434	0.13	18,890	0.40	4769	0.10
	ROI4	5856	0.50	13,995	1.20	4423	0.38
	ROI5	8026	0.26	17,911	0.59	6099	0.20
PC(16:0/16:0)	Whole brain	4594	1.76	4265	1.63	5883	2.25
	ROI1	2357	0.03	2063	0.03	2999	0.04
	ROI2	4909	0.63	2063	0.58	6474	0.83
	ROI3	4803	0.10	4545	0.11	6063	0.13
	ROI4	4164	0.36	3531	0.30	5143	0.44
	ROI5	4484	0.15	4321	0.14	6367	0.21

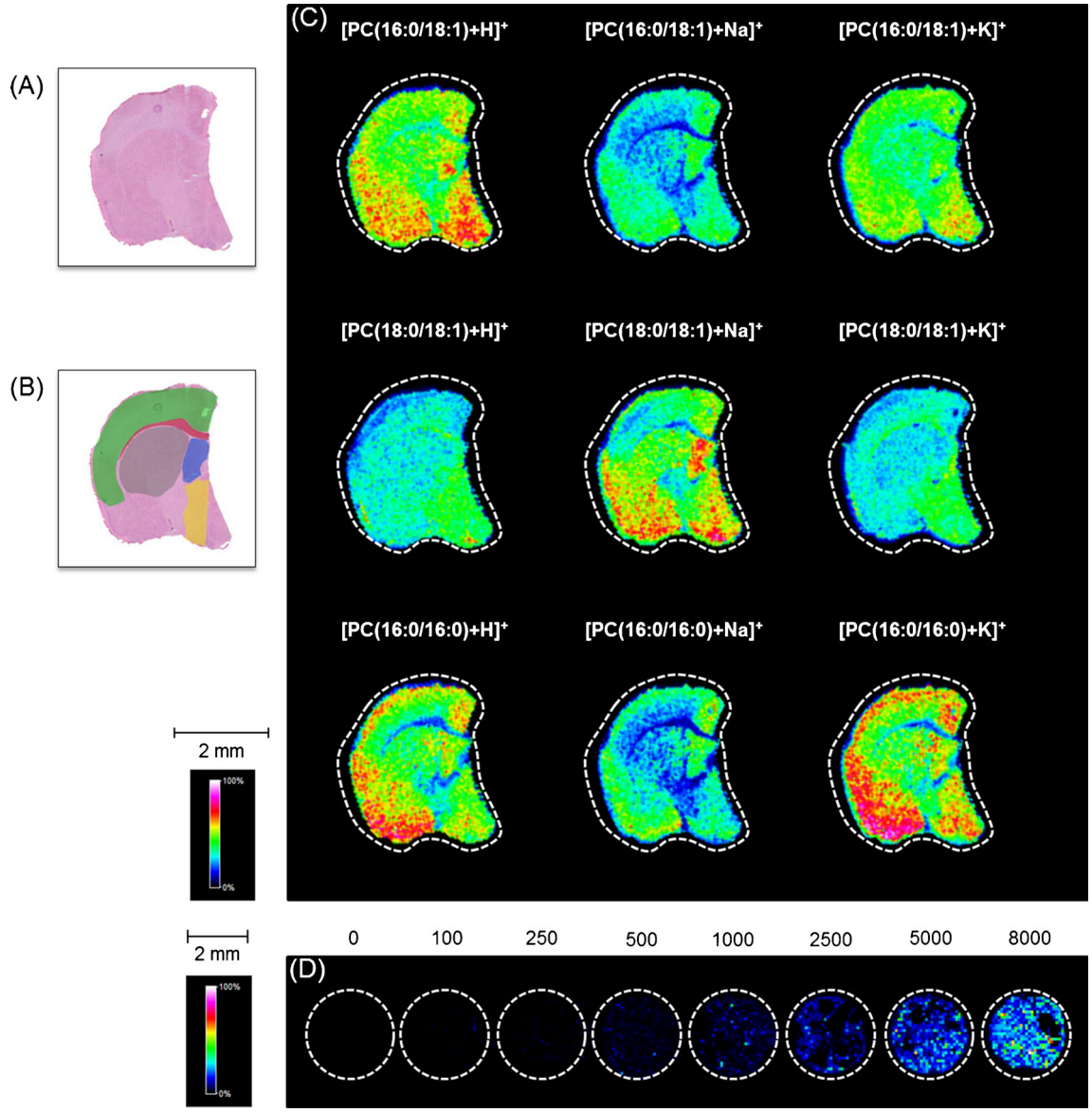

Fig. 6 Analysis by MALDI MSI of sections from an intact brain and brain homogenates spiked with a range of PC(16:0 d31/18:1) concentrations. (**A**) A serial section after H&E staining. (**B**) Definition of ROIs on the section (ROI1: *red* corpus callosum; ROI2: *green* cerebral cortex; ROI3: *blue* lateral septal nucleus; ROI4: *grey* caudoputamen; ROI5: *yellow* hypothalamus). (**C**) Molecular images showing the distribution of different PC ionic species ($[M+H]^+$, $[M+Na]^+$ and $[M+K]^+$) across the intact brain section surface. (**D**) Molecular image showing the intensity scale corresponding to the $[PC(16:0\ d31/18:1)+H]^+$ on the spiked (between 100 and 8000 μg/g) homogenate sections analysed simultaneously to the intact brain

supplementary material, Table S-3). These data were consistent with the quantitative results generated from non-normalized data set found in this work.

Conclusions

In this study, endogenous PCs were quantified in the brain section using MALDI MSI. The approach was based on the simultaneous analysis of sections from an intact brain and brain homogenates spiked with different PC(16:0 d31/18:1) concentrations. The quantitative information extracted from MALDI MSI data was consistent with values found in the literature. In the next future, orthogonal methods may be developed to corroborate these data such as classical extraction followed by liquid chromatography mass spectrometry quantitative analysis.

The reported approach has the advantage that the standard and the analyte have a similar molecular structure, while being present in a similar environment. This

ensures that both compounds behaved in the same way during all the MALDI MSI processes. However, in some cases, tissue structures may have different chemical and morphological environments. During a MALDI MSI analysis, these are likely to have different suppressive effects on the PC signals. In this context, it would be more appropriate to use homogenates prepared from specific structures of a tissue, corresponding to given ROIs defined in molecular images. Their specific effects will thus be taken into account. However, depending on the structure and the tissue of interest, it may be difficult to collect these samples. In the same way, some control biological samples (e.g. from cancer research) may lack the preparation of homogenates. The incorporation of the standard using a spraying method would be an interesting alternative to the use of tissue homogenates. Serial non-homogenized tissue sections may be spiked (by spraying) with different standard concentrations. Calibration curves may then be generated for different ROIs defined on a tissue section. Finally, a lipid of interest may be quantified in different ROIs using these "ROI-specific" calibration curves. In this way, this approach would probably be more simple and universal, while requiring a less control sample. It may also address the eventual problems of ion suppression effects, which may be specific to different ROIs. However, a careful optimization of a spraying approach will be mandatory in order to ensure that the standard acts like the endogenous analyte during the MALDI MSI process. Tissue homogenates would then be very useful to optimize spraying conditions for controlling that the standard sprayed on a tissue homogenate surface closely mimics the standard incorporated to a tissue homogenate during the homogenization process. Respecting this condition, such a spray-based approach may be a good way to quantify endogenous compounds within a large range of tissues. Quantification by MALDI MSI may then find many applications in the fields of biology, histopathology and pharmacology.

The work reported here opens new prospects concerning the quantification of small endogenous compounds within tissue sections. It represents the promising first step towards the quantification of lipids by MALDI MSI. It now requires further efforts in order to develop a more universal quantitative method.

Acknowledgments L. J. thanks the REFRACT project for funding ("Action de Recherche Concertée," ULg, Belgium). R. L. is a postdoc fellow of the ULg Research Council. The FTMS instrument was acquired with European Funds for Regional Development (FEDER) and the FNRS.

Conflict of interest The authors have declared no conflict of interest.

References

1. Zemski Berry KA, Hankin JA, Barkley RM, Spraggins JM, Caprioli RM, Murphy RC (2011) MALDI imaging of lipid biochemistry in tissues by mass spectrometry. Chem Rev 111(10):6491–6512
2. Santos CR, Schulze A (2012) Lipid metabolism in cancer. FEBS J 279(15):2610–2623
3. Abrass CK (2004) Cellular lipid metabolism and the role of lipids in progressive renal disease. Am J Nephrol 24(1):46–53
4. Lee CH, Olson P, Evans RM (2003) Minireview: lipid metabolism, metabolic diseases, and peroxisome proliferator-activated receptors. Endocrinology 144(6):2201–2207
5. Frisardi V, Panza F, Seripa D, Farooqui T, Farooqui AA (2011) Glycerophospholipids and glycerophospholipid-derived lipid mediators: a complex meshwork in Alzheimer's disease pathology. Prog Lipid Res 50(4):313–330
6. Paradisi G, Ianniello F, Tomei C, Bracaglia M, Carducci B, Gualano MR, La Torre G, Banci M, Caruso A (2010) Longitudinal changes of adiponectin, carbohydrate and lipid metabolism in pregnant women at high risk for gestational diabetes. Gynecol Endocrinol 26(7):539–545
7. Giannopoulos PF, Joshi YB, Praticò D (2014) Novel lipid signaling pathways in Alzheimer's disease pathogenesis. Biochem Pharmacol 88(4):560–564
8. Gode D, Volmer DA (2013) Lipid imaging by mass spectrometry—a review. Analyst 138(5):1289–1315
9. Goto T, Terada N, Inoue T, Nakayama K, Okada Y, Yoshikawa T, Miyazaki Y, Uegaki M, Sumiyoshi S, Kobayashi T, Kamba T, Yoshimura K, Ogawa O (2014) The expression profile of phosphatidylinositol in high spatial resolution imaging mass spectrometry as a potential biomarker for prostate cancer. PLoS One 9(2):e90242
10. Veloso A, Fernández R, Astigarraga E, Barreda-Gómez G, Manuel I, Giralt MT, Ferrer I, Ochoa B, Rodríguez-Puertas R, Fernández JA (2011) Distribution of lipids in human brain. Anal Bioanal Chem 401(1):89–101
11. Thomas A, Charbonneau JL, Fournaise E, Chaurand P (2012) Sublimation of new matrix candidates for high spatial resolution imaging mass spectrometry of lipids: enhanced information in both positive and negative polarities after 1,5-diaminonapthalene deposition. Anal Chem 84(4):2048–2054
12. Kawashima M, Iwamoto N, Kawaguchi-Sakita N, Sugimoto M, Ueno T, Mikami Y, Terasawa K, Sato TA, Tanaka K, Shimizu K, Toi M (2013) High-resolution imaging mass spectrometry reveals detailed spatial distribution of phosphatidylinositols in human breast cancer. Cancer Sci 104(10):1372–1379
13. Berry KAZ, Gordon WC, Murphy RC, Bazan NG (2014) Spatial organization of lipids in the human retina and optic nerve by MALDI imaging mass spectrometry. J Lipid Res 55(3):504–515
14. Dyer JM, Deb-Choudhury S, Cornellison CD, Krsinic G, Dobbie P, Rosenvold K, Clerens S (2014) Spatial and temporal mass spectrometric profiling and imaging of lipid degradation in bovine M. longissimus dorsi lumborum. J Food Compos Anal 33(2):203–209
15. Wang HYJ, Wu HW, Tsai PJ, Liu CB, Zheng ZF (2014) Matrix-assisted laser desorption/ionization mass spectrometry imaging of cardiolipins in rat organ sections. Anal Bioanal Chem 406(2):565–575
16. Matsumoto J, Sugiura Y, Yuki D, Hayasaka T, Goto-Inoue N, Zaima N, Kunii Y, Wada A, Yang Q, Nishiura K, Akatsu H, Hori A, Hashizume Y, Yamamoto T, Ikemoto K, Setou M, Niwa SI (2011) Abnormal phospholipids distribution in the prefrontal cortex from a patient with schizophrenia revealed by matrix-assisted laser desorption/ionization imaging mass spectrometry. Anal Bioanal Chem 400(7):1933–1943
17. Arafah K, Longuespee R, Desmons A, Kerdraon O, Fournier I, Salzet M (2014) Lipidomics for clinical diagnosis: dye-assisted laser

desorption/ionization (DALDI) method for lipids detection in MALDI mass spectrometry imaging. Omics: J Integr Biol. doi:10.1089/omi.2013.0175
18. Sparvero LJ, Amoscato AA, Dixon CE, Long JB, Kochanek PM, Pitt BR, Bayir H, Kagan VE (2012) Mapping of phospholipids by MALDI imaging (MALDI-MSI): realities and expectations. Chem Phys Lipids 165(5):545–562
19. Cimino J, Calligaris D, Far J, Debois D, Blacher S, Sounni NE, Noel A, De Pauw E (2013) Towards lipidomics of low-abundant species for exploring tumor heterogeneity guided by high-resolution mass spectrometry imaging. Int J Mol Sci 14(12):24560–24580
20. Ellis SR, Bruinen AL, Heeren RMA (2014) A critical evaluation of the current state-of-the-art in quantitative imaging mass spectrometry. Anal Bioanal Chem 406(5):1275–1289
21. Pirman DA, Yost RA (2011) Quantitative tandem mass spectrometric imaging of endogenous acetyl-L-carnitine from piglet brain tissue using an internal standard. Anal Chem 83(22):8575–8581
22. Takai N, Tanaka Y, Inazawa K, Saji H (2012) Quantitative analysis of pharmaceutical drug distribution in multiple organs by imaging mass spectrometry. Rapid Commun Mass Spectrom 26(13):1549–1556
23. Hamm G, Bonnel D, Legouffe R, Pamelard F, Delbos JM, Bouzom F, Stauber J (2012) Quantitative mass spectrometry imaging of propranolol and olanzapine using tissue extinction calculation as normalization factor. J Proteomics 75(16):4952–4961
24. Pirman DA, Reich RF, Kiss A, Heeren RMA, Yost RA (2013) Quantitative MALDI tandem mass spectrometric imaging of cocaine from brain tissue with a deuterated internal standard. Anal Chem 85(2):1081–1089
25. Nilsson A, Fehniger TE, Gustavsson L, Andersson M, Kenne K, Marko-Varga G, Andrén PE (2010) Fine mapping the spatial distribution and concentration of unlabeled drugs within tissue microcompartments using imaging mass spectrometry. PLoS One 5(7): e11411
26. Groseclose MR, Castellino S (2013) A mimetic tissue model for the quantification of drug distributions by MALDI imaging mass spectrometry. Anal Chem 85(21):10099–10106
27. Takai N, Tanaka Y, Saji H (2014) Quantification of small molecule drugs in biological tissue sections by imaging mass spectrometry using surrogate tissue-based calibration standards. Mass Spectrom 3(1):A0025
28. Koeniger SL, Talaty N, Luo Y, Ready D, Voorbach M, Seifert T, Cepa S, Fagerland JA, Bouska J, Buck W, Johnson RW, Spanton S (2011) A quantitation method for mass spectrometry imaging. Rapid Commun Mass Spectrom 25(4):503–510
29. Hankin JA, Murphy RC (2010) Relationship between MALDI IMS intensity and measured quantity of selected phospholipids in rat brain sections. Anal Chem 82(20):8476–8484
30. Landgraf RR, Garrett TJ, Prieto Conaway MC, Calcutt NA, Stacpoole PW, Yost RA (2011) Considerations for quantification of lipids in nerve tissue using matrix-assisted laser desorption/ionization mass spectrometric imaging. Rapid Commun Mass Spectrom 25(20):3178–3184
31. Hankin JA, Barkley RM, Murphy RC (2007) Sublimation as a method of matrix application for mass spectrometric imaging. J Am Soc Mass Spectrom 18(9):1646–1652
32. Carter CL, McLeod CW, Bunch J (2011) Imaging of phospholipids in formalin fixed rat brain sections by matrix assisted laser desorption/ionization mass spectrometry. J Am Soc Mass Spectrom 22(11): 1991–1998
33. Jackson SN, Wang HYJ, Woods AS (2005) Direct profiling of lipid distribution in brain tissue using MALDI-TOFMS. Anal Chem 77(14):4523–4527
34. Jackson SN, Wang HYJ, Woods AS, Ugarov M, Egan T, Schultz JA (2005) Direct tissue analysis of phospholipids in rat brain using MALDI-TOFMS and MALDI-ion mobility-TOFMS. J Am Soc Mass Spectrom 16(2):133–138
35. Mikawa S, Suzuki M, Fujimoto C, Sato K (2009) Imaging of phosphatidylcholines in the adult rat brain using MALDI-TOF MS. Neurosci Lett 451(1):45–49
36. Deininger SO, Cornett DS, Paape R, Becker M, Pineau C, Rauser S, Walch A, Wolski E (2011) Normalization in MALDI-TOF imaging datasets of proteins: practical considerations. Anal Bioanal Chem 401(1):167–181
37. Barnard T (1987) Rapid freezing techniques and cryoprotection of biomedical specimens. Scanning Microsc 1(3):1217–1224
38. Krafft C, Sobottka SB, Schackert G, Salzer R (2005) Near infrared Raman spectroscopic mapping of native brain tissue and intracranial tumors. Analyst 130(7):1070–1077
39. Dreissig I, Machill S, Salzer R, Krafft C (2009) Quantification of brain lipids by FTIR spectroscopy and partial least squares regression. Spectrochim Acta Part A Mol Biomol Spectrosc 71(5):2069–2075
40. Herculano-Houzel S (2009) The human brain in numbers: a linearly scaled-up primate brain. Front Human Neurosci 3:1–11
41. Petković M, Schiller J, Müller M, Benard S, Reichl S, Arnold K, Arnhold J (2001) Detection of individual phospholipids in lipid mixtures by matrix-assisted laser desorption/ionization time-of-flight mass spectrometry: phosphatidylcholine prevents the detection of further species. Anal Biochem 289(2):202–216